Oxidized detonation nanodiamonds act as an efficient metal-free photocatalyst to produce hydrogen under solar irradiation

Clément Marchal, Lorris Saoudi, Hugues A Girard, Valérie Keller, Jean-charles Arnault

ADVANCED ENERGY & SUSTAINABILITY RESEARCH
Open Access
www.advenergysustres.com

Oxidized Detonation Nanodiamonds Act as an Efficient Metal-Free Photocatalyst to Produce Hydrogen Under Solar Irradiation

*Clément Marchal, Lorris Saoudi, Hugues A. Girard, Valérie Keller, and Jean-Charles Arnault**

Herein, it is revealed for the first time that oxidized detonation nanodiamonds (Ox-DND) can produce hydrogen under solar irradiation without addition of cocatalyst or formation of heterojunction with another semiconductor. This hydrogen production is investigated using two sacrificial reagents and compared to the one of hydrogenated detonation nanodiamonds (H-DND). The effect of the Ox-DND and sacrificial reagent concentrations on the hydrogen production is also studied. At its maximum, a H_2 production yield of 32 µmol h^{-1} is obtained for a Ox-DND concentration of 12.5 µg mL^{-1} (using only 1 vol% of triethanolamine as sacrificial reagent), similar to the one of TiO_2 nanoparticles tested at the same concentration in the same illumination conditions.

1. Introduction

Nanodiamond (ND) inherits the most outstanding properties of bulk diamond: high Young modulus and weak friction coefficient, semiconductor behavior, thermal conductivity, versatile carbon-based surface chemistry, photoluminescent color centers, and biocompatibility.[1] Accordingly, they are actively investigated for nanomedicine, quantum technologies, advanced composites, and lubricants. ND is also seriously considered toward catalysis and energy-related applications. An interesting catalytic activity of surface graphitized ND for dehydrogenation reactions was reported[2] while Shao et al. evidenced very promising oxidation properties toward organic pollutants remediation.[3] Toward photocatalysis, one previous study by Zhang et al. also suggested a photocatalytic behavior of hydrogenated ND for the CO_2 reduction into CO under UV illumination.[4] In the same idea, Maza et al. recently reported on the degradation of fluorinated compounds by UV-illuminated hydrogenated NDs.[5] For photo-catalyzed hydrogen production, literature only reports on few studies dealing with the combination of NDs with other photocatalysts like g-C_3N_4[6] or Cu_2O.[7] However, with ND as a single photocatalyst, only Jang et al. measured hydrogen produced by water splitting[8] but with the help of an intense laser irradiation at 532 nm and furthermore using hydrogenated ND.

This work focuses on NDs produced by detonation process.[9] Such detonation nanodiamonds (DND) behave in nanometric sizes (2–10 nm) and present a defective diamond core with structural defects like stacking faults, twins, or vacancies.[10] Different surface treatments (gas phase or wet chemistry) were developed to remove the sp^2 or amorphous carbon from DND surface and to promote a homogeneous surface chemistry via oxidation,[11] hydrogenation,[12] or surface graphitization.[13] Such surface modifications are important first steps before the grafting of moieties of interest, especially for bioapplications.[14] The nature of the functional surface groups will significantly influence the chemicophysical properties of DND like their electronic structure,[15] their colloidal properties in water,[16,17] or their behavior under irradiation.[18]

The present study reveals that hydrogen production is allowed from aqueous suspensions of oxidized detonation nanodiamonds (Ox-DND) even under broad and moderate solar illumination without any cocatalyst and with low/moderate concentrations of sacrificial reagents (triethanolamine, TEOA or methanol, MeOH). It is to the best of our knowledge the first report for DND in these conditions. When the surface chemistry of DND is tuned to hydrogenated one, there is no more hydrogen produced in comparison with the sacrificial reagent alone.

2. Results

2.1. DND Surface Chemistry

The oxygen atomic concentration measured by XPS on Ox-DND is 9.9 at%, in agreement with the literature data after such treatment.[19] For H-DND, a residual oxygen concentration of 2.7 at% is obtained (Table S1, Supporting Information). Apart from

C. Marchal, V. Keller
ICPEES
CNRS/University of Strasbourg
UMR 7515, 67000 Strasbourg, France
L. Saoudi, H. A. Girard, J.-C. Arnault
Université Paris-Saclay, CEA, CNRS, NIMBE
91191 Gif sur Yvette, France
E-mail: jean-charles.arnault@cea.fr
The ORCID identification number(s) for the author(s) of this article can be found under https://doi.org/10.1002/aesr.202300260.

DOI: 10.1002/aesr.202300260

carbon and oxygen, only nitrogen was detected by XPS, with an atomic concentration between 1.5 and 1.8 at%, as it is expected for ND synthesized by detonation (nitrogen mainly located in the ND core).[20] Thus, other possible chemical impurities may have atomic concentrations lower than 0.5 at%.[19] A fine analysis of carbon core levels (C 1*s*) reveals significant differences in binding states of carbon for both DND (**Figure 1**). The repartition of the different contributions in terms of percentages of C 1*s* surface area is reported in Table S2, Supporting Information. The component related to sp^3 carbon is located at 285.9 eV for both DND. A specific signature of DND related to structural defects and C—N bonds is present at +0.8 eV from sp^3 carbon. As already described elsewhere,[13] the balance between the sp^3 carbon and structural defects evolves from Ox-DND to H-DND, toward higher proportion of diamond carbon after annealing under H_2. Then, components related to C—O—R (alcohols and/or etheric bridges), C═O, and COOH bonds are located at 1.7, 2.6, and 3.7 eV from sp^3 carbon, respectively. After hydrogenation, these components tend to decrease. For Ox-DND, an additional component is detected at −1.5 eV from sp^3 carbon representing 3.7 % of the total carbon area. According to our previous work on graphitized DND, such a contribution may be assigned to sp^2 carbon.[13] This component is not detected for H-DND.

Valence bands of Ox-DND and H-DND are compared in **Figure 2**. Both surface chemistries exhibit two contributions at ≈15 and 18.5 eV, assigned to sp^3 carbon and C 2*s*, respectively. For Ox-DND, a prominent O 2*s* peak is observed in coherence with the oxygen concentration of 9.9 at%. A feature is also clearly detected at 10 eV for Ox-DND, previously attributed to nondiamond carbon.[21] This later result is in line with the XPS analysis of the C 1*s* core level (Figure 1). Considering these spectra, no energy shift is evidenced between both DND when tuning the DND surface chemistry from oxidized to hydrogenated. This is a major difference compared to milled ND for which of an energy downshift of 2.3 eV was reported for hydrogenated ND compared to oxidized ones.[22]

The surface chemistry of each DND was also investigated using FTIR, spectra of H- and Ox-DND are provided in **Figure 3**a. For Ox-DND, the spectrum reveals the presence of C═O stretching modes (1800 cm^{-1}) related to carboxylic acids or anhydrides and a large band located between 950 and 1280 cm^{-1} mainly attributed to C—O stretching modes linked to alcohols, esters, and epoxy features on these oxidized DND. A shouldering also occurs between 3000 and 3500 cm^{-1} related to O—H stretching modes linked to carboxylic acids and water residues.[23]

For H-DND, a reduction of the "C═O" and "C—O" related bands occurs, which reveals the desorption of carbon–oxygen functions from the surface, in agreement with XPS results. At the same time, a clear signature of C—H terminations appears, with two intense peaks located at 2940 and 2870 cm^{-1} related to C—H stretching modes.[23] A large band from 1700 to 1550 cm^{-1} is also visible on H-DND spectrum. Several components may take place in this area and contribute to this band, including residues of carbonyls stretching modes (1670 cm^{-1}), OH bending modes, and C═C stretching modes resulting from reconstructions at the surface of H-DND.[24] The peak located at 1330 cm^{-1} is assigned to C—C diamond lattice made visible in FTIR due to substitutional nitrogen incorporated during the

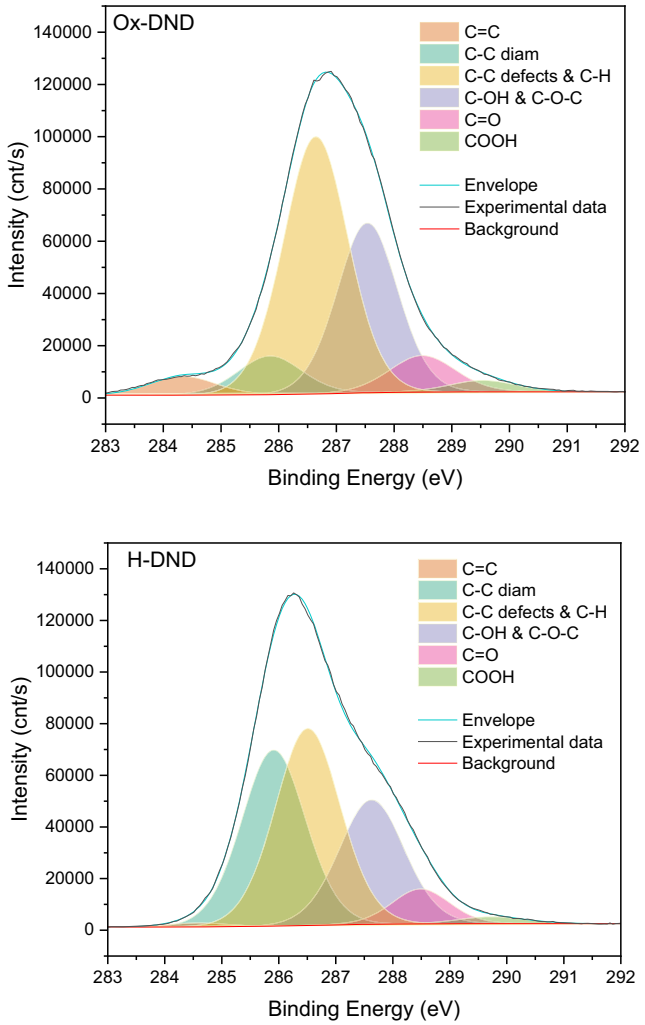

Figure 1. C 1s core level spectra of Ox-DND (top) and H-DND (bottom).

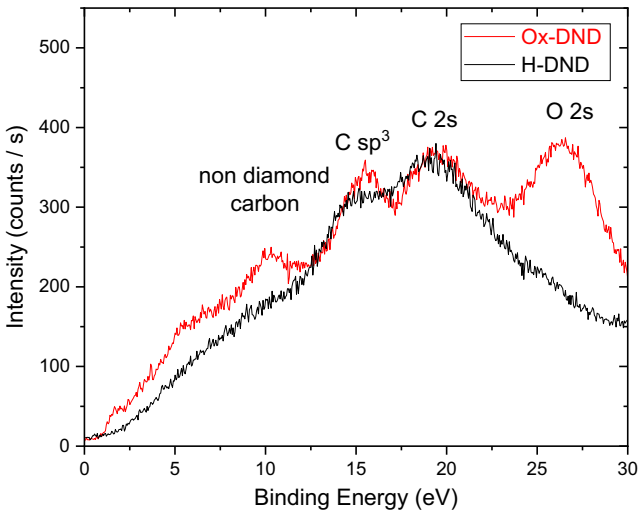

Figure 2. Valence band spectra of Ox-DND and H-DND.

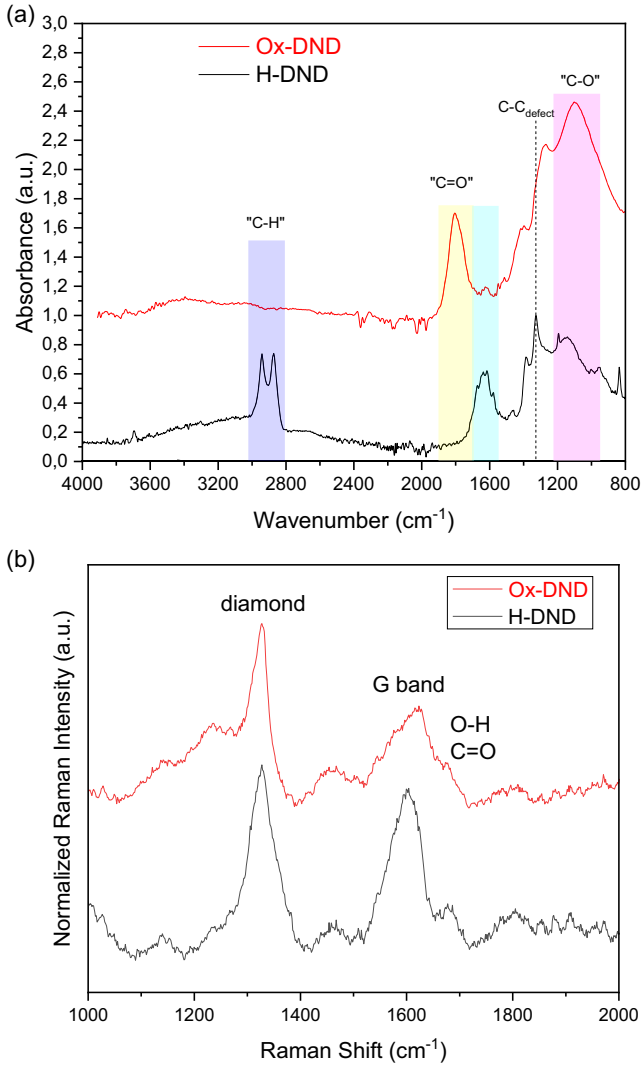

Figure 3. a) FTIR and b) Raman spectra of Ox-DND and H-DND.

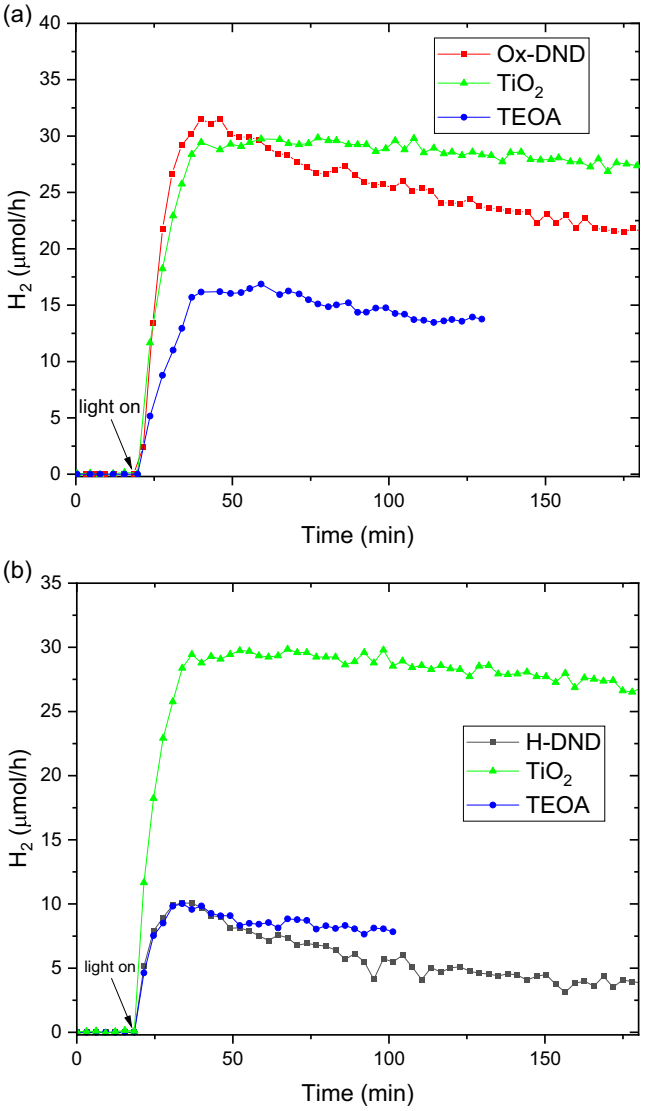

Figure 4. Hydrogen production rate for a) Ox-DND (red squares) (TEOA: 1 vol%). TiO_2 P25 (green triangles) and TEOA (blue circles) references were added for comparison. 10 mg of Ox-DND and TiO_2 were used, corresponding to a concentration of 12.5 µg mL^{-1}; b) for H-DND (black squares) (TEOA: 1 vol%). TiO_2 P25 (green triangles) and TEOA (blue circles) references measured in the same conditions were added for comparison. The amount of both photocatalysts is 10 mg, corresponding to a concentration of 12.5 µg mL^{-1}.

detonation synthesis (1.5–2 at% according to XPS measurements).[25] Hidden by the carbon–oxygen stretching modes on Ox-DND spectrum, this peak is revealed after their desorption and signs for diamond core of DND.

Ox-DND and H-DND were then characterized by Raman spectroscopy (Figure 3b). Both surface chemistries exhibit a quite similar Raman signature, with a first-order diamond peak lying at 1328 cm^{-1}, red-shifted, and asymmetric compared to bulk diamond as expected for DND.[26] The broad band visible on both samples between 1500 and 1700 cm^{-1} corresponds to the overlapping of carbon G band usually located at 1590 cm^{-1}, OH bending modes at 1640 cm^{-1}, and C=O stretching modes around 1700 cm^{-1}.

2.2. Photocatalytic Experiments

2.2.1. Effect of DND Surface Chemistry on Hydrogen Production

Typical profiles showing the kinetic of hydrogen generation versus time are presented on **Figure 4**a for 10 mg of Ox-DND with a TEOA content of 1 vol%. A direct comparison with literature values of H_2 production rate is always complicated since nature and concentration of antioxidant may differ, as well as the concentration of photocatalyst or the illumination conditions. Thus, the hydrogen production rate of the same amount of commercial TiO_2 particles (P25, Evonik) suspended in ultra-pure water in presence of TEOA (1 vol%) and illuminated in similar conditions is compared to Ox-DND, as shown in Figure 4a. The same experimental conditions were also applied to TEOA alone during slightly shorter duration.

When illumination is turned on, a rising H_2 yield is detected with the same slope whatever the photocatalyst (Ox-DND and TiO_2) assuming to be due to transfer of the gas-reaction product from reaction medium to analysis. Even if TEOA is present at low concentration, it also contributes to a weaker H_2 production (up to 16 μmol h^{-1} after stabilization) that cannot be attributed to water splitting. Indeed, it corresponds to the photo reforming of alcohol functions and/or to the deprotonation of tertiary amines. One can also observe the similar maxima of production reached after 20 min, around 30 and 32 μmol h^{-1} on TiO_2 P25 and Ox-DND materials, respectively. Then a quasi-stabilization of the H_2 production yield is observed for TiO_2 while a clear decrease of this production yield is observed for Ox-DND (−27% after 150 min). Here, an evolution of the Ox-DND surface sites due to the presence at their neighboring of the light-generated radical species may be considered as impacting stability. Furthermore, repeatability measurements performed on four independent batches of Ox-DND (Figure S4, Supporting Information) showed relative experimental error of ≈10% on evolved hydrogen production rate. Nevertheless, this experiment evidences for the first time that Ox-DND alone can act as a photocatalyst for the generation of H_2 at the same level of initial H_2 production than the reference TiO_2 P25 even under solar light illumination, without the help of any cocatalyst and a low concentration of sacrificial agent. The H_2 production yield of 23 μmol h^{-1} for 10 mg of Ox-DND obtained after 200 min is close to the ones generally reported by the literature for isolated nanomaterials.[27]

A similar experiment was performed using H-DND. Corresponding data displayed on Figure 4b reveal in this case an inhibiting behavior in hydrogen overproduction. Indeed, the measured hydrogen content is very close to the TEOA reference (10 μmol h^{-1}). In the same experimental conditions, a maximum hydrogen production of 30 μmol h^{-1} is obtained for TiO_2 P25 revealing additional hydrogen production. The evolution of produced hydrogen with time exhibits a decreasing trend for both photocatalysts: −16% and −55% after 150 min, for TiO_2 and H-DND, respectively.

2.2.2. Effects of Ox-DND and TEOA Concentrations on Hydrogen Production

The influence of Ox-DND concentration on the hydrogen production was then investigated for a TEOA content of 1 vol% (**Figure 5**a). Very similar maxima of hydrogen production rate, 26 and 27 μmol h^{-1}, are obtained for 5 and 10 mg of DND-Ox, respectively, after 18 and 22 min of solar illumination. For the lowest Ox-DND loading, this corresponds to a hydrogen production rate of 5.2 mmol h^{-1} g^{-1}. At the highest Ox-DND loading (20 mg), the H_2 production rate dropped to 20 μmol h^{-1} (i.e., 1 mmol h^{-1} g^{-1}) at its maximum, probably due to a light screening effect of suspended DND.

The influence of the sacrificial reagent concentration during the illumination was also investigated (Figure 5b), as it partially contributes to H_2 production. Concentration of TEOA was then varied from 0.1 to 1 vol%. As expected, the more concentrated in TEOA were the suspensions, the more efficient was the H_2 generation for a similar concentration of DND-Ox. However, one can highlight that the H_2 production is not proportional to TEOA

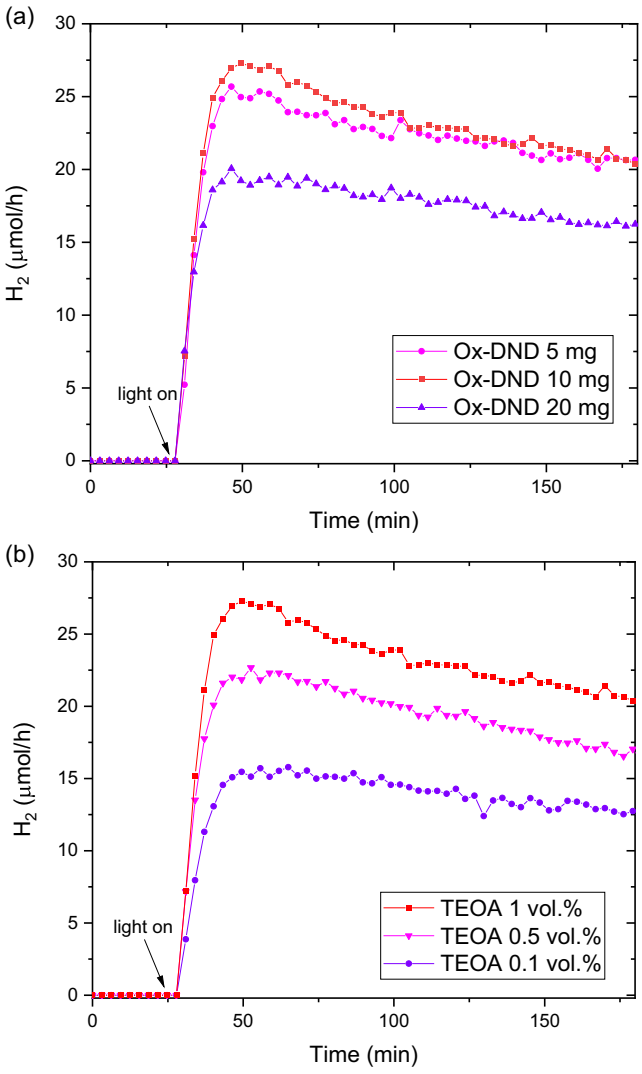

Figure 5. Hydrogen production rate (μmol h^{-1}) a) for different contents of Ox-DND: 5 (pink circles), 10 (red squares) or 20 mg (purple triangles) in aqueous suspension corresponding to concentrations of 6.25, 12.5, and 25 μg mL^{-1}, respectively. TEOA at 1 vol% is used as sacrificial reagent; b) for 10 mg of Ox-DND (corresponding to 12.5 μg mL^{-1}) at different TEOA concentrations: 0.1 vol% (purple circles), 0.5 vol% (pink triangles), and 1 vol% (red squares).

concentration, confirming that major H_2 production is the result of Ox-DND. Maxima of hydrogen production are 27, 23 and 16 μmol h^{-1} for TEOA concentrations of 1, 0.5, and 0.1 vol%, respectively. Concerning the stability of the production, whatever the TEOA concentration, H_2 yield reached a maximum after 22 to 27 min of illumination followed by a continuous decrease (between −18% and −22%), also confirming the same assumption than aforementioned.

2.2.3. Effect of the Sacrificial Reagent on the Hydrogen Production

Performances of Ox-DND and H-DND were then measured using MeOH as an alternative sacrificial reagent. At MeOH

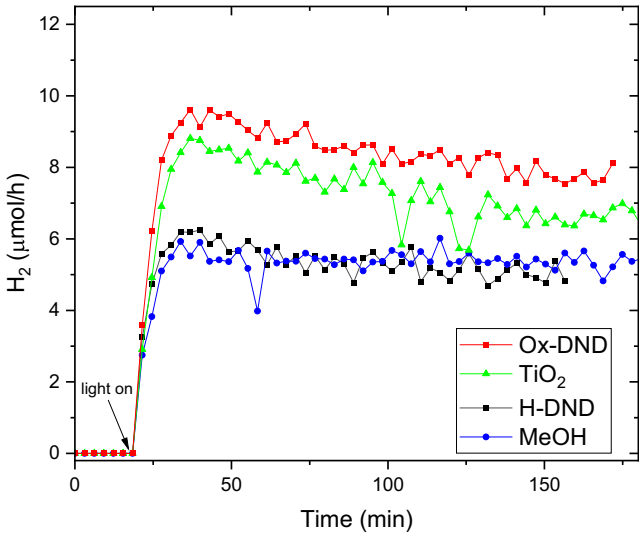

Figure 6. Hydrogen production rate (µmol h^{-1}) for Ox-DND (red squares) and H-DND (black squares) in water with MeOH 10 vol%. MeOH 10 vol% (blue squares) and TiO_2 P25 (green triangles) references were measured in the same conditions. The content of photocatalysts is 10 mg.

1 vol%, H_2 amount close to the µ-GC detection limit was obtained (3 µmol h^{-1}) whatever the surface chemistry of DND.

When MeOH concentration is increased up to 10 vol% (**Figure 6**), Ox-DND led to a H_2 amount close to 10 µmol h^{-1}, exceeding the one of MeOH reference (6 µmol h^{-1}) and comparable to TiO_2 (9 µmol h^{-1}). Here as well, the hydrogen production rate tends to decrease with time. After 150 min, it has lost 19%. As with TEOA, in presence of H-DND, the produced hydrogen amount is comparable to the one obtained for the MeOH reference.

3. Discussion

A hydrogen production is evidenced for oxidized DND under solar illumination whatever the sacrificial reagent. A maximum hydrogen production rate of 26 µmol h^{-1}, i.e., 5.2 mmol h^{-1} g^{-1}, is reached when only 5 mg of Ox-DND are dispersed in 800 mL of water (6.25 µg mL^{-1}). This maximum H_2 production, obtained with Ox-DND alone, without cocatalyst, is very competitive compared to other carbon-based photocatalysts. For instance, 200 µmol h^{-1} g^{-1} were obtained with Au(0.5 wt%)/g-C_3N_4, investigated in the same photocatalytic conditions.[27] However, when the same experiment is performed with hydrogenated DND from the same origin, the hydrogen overproduction is no more observed. Therefore, two main questions have to be discussed at this stage: 1) why Ox-DND allow hydrogen production and not H-DND? 2) how DND are able to absorb visible light while diamond is a wide bandgap semiconductor (5.47 eV)?

Let us now discuss the origin of the hydrogen production under solar illumination only observed for Ox-DND whatever the sacrificial reagent, and not for H-DND. Both types of nanoparticles are produced from the same initial raw powder. Even more, H-DND is prepared by the hydrogenation (750 °C under H_2 at atmospheric pressure) of Ox-DND. Therefore, they only differ by an additional annealing at high temperature for H-DND and the nature of their surface terminations. Regarding light absorption, both types of ND have very similar UV–vis absorption spectra (Figure S7, Supporting Information). Thus, the photoreactivity of Ox-DNDs does not seem to arise from differences in light absorption. On bulk diamond, it is known that surface chemistry strongly affects the band diagram, with a shift of several eV toward higher energies of the conduction and valence bands for hydrogenated material. Very recently, a study from Rezek team confirmed experimentally that this shift is preserved at the nanoscale, even for DND.[28] A difference of 1.3 eV in the conduction and valence band positions is measured between both surface chemistries (**Scheme 1**). Furthermore, in the same study, authors confirm by optical measurements that the bandgap remains similar for Ox-DND and H-DND. As our oxidation and hydrogenation conditions are similar to those of Rezek study, we may consider that our Ox-DND and H-DND encounter the same band alignments and shifts. The different reactivity of Ox-DND and H-DND toward H_2 production may thus result from this modification of the DND band diagram after hydrogenation. For sake of clarity, we build the band diagrams of Scheme 1, adapted from Rezek study[28] for the DND and from Jimenez–Calvo study[29] for TiO_2. This representation highlights the lower energy position of the Ox-DND valence band, which may favor the water oxidation, source of H^+, compared to H-DND.

Beyond the nature of chemical groups at their surface which plays on the band diagram, we also measured by XPS that Ox-DND behaves almost 4% of sp^2 hybridized carbon on their surface. After hydrogenation, this sp^2 carbon vanishes. Here is another difference in terms of surface chemistry, which needs to be considered in the light of the recent spectroscopic investigation which demonstrated the production of solvated electrons under visible light (400 nm) by hydrogen plasma-treated DND that contained sp^2 carbon.[30] Intermediate states in the bandgap

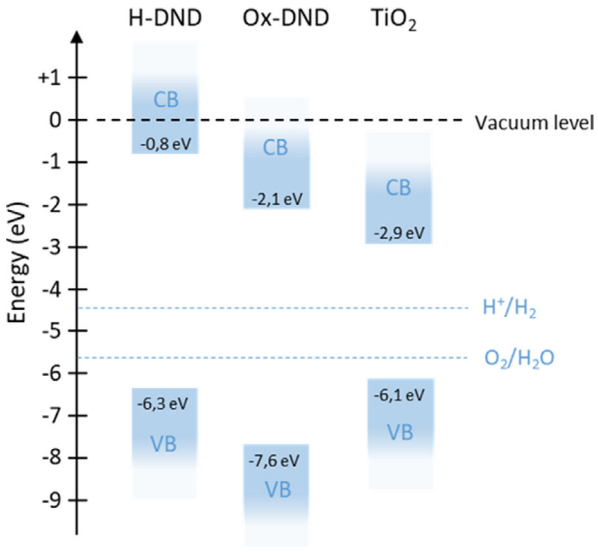

Scheme 1. Band diagrams of H-DND, Ox-DND, and P25 TiO_2 obtained by experimental measurements, adapted from Miliaieva et al.[28] and Jimenez-Calvo et al.[29]

linked to this sp^2 carbon may favor on Ox-DND charge separation and charge transfer.

Ox-DND and H-DND also differ by their hydrophilicity. If both types of DND can be dispersed in water, a particular arrangement of water molecules surrounding H-DND (which are natively hydrophobic as bulk hydrogenated diamond) was evidenced by several spectroscopic investigations of aqueous suspensions.[16,31] These studies revealed a different hydrogen bond network around H-DND compared to Ox-DND. A weaker hydrogen bonding occurs between adjacent water molecules at the H-DND/water interface, resulting in a specific water layer that straddle the interface between the water and hydrophobic surface of H-DND. As the adsorption of water molecules on the photocatalyst surface is a key step for the hydrogen production, this difference between Ox-DND and H-DND water interfaces is worth to consider to discuss our results.

Now that we highlighted the main differences between Ox-DND and H-DND that may explain their opposite reactivity toward H_2 production, let us now discuss on how DND are able to absorb visible light. NDs produced by detonation are known to be highly defective, containing structural defects (twins and stacking faults)[10] and chemical impurities like nitrogen originating from the detonation process (up to 1.8 at% in our case, see Table S1, Supporting Information). To investigate the potential effect of these defects in visible light absorption, we performed similar oxidation and hydrogen treatments on NDs produced by the milling of synthetic diamond (MND). Experimental conditions of both surface treatments as well as XPS, FTIR, and high-resolution transmission electron microscopy characterizations of these Ox- and H-MND were elsewhere reported.[22] Compared to DND, these MND particles exhibit an excellent crystalline quality (with facets) and no nitrogen (up to the XPS detection limit of few 0.1 at%). According to XPS data, the oxygen concentration of Ox-MND is very close to the one of Ox-DND (9.4 at% and 9.9 at%, respectively) and both ND contains a comparable amount of sp^2 carbon (4% of the C 1*s* area). For hydrogenated particles, we measured 1 at% of oxygen remaining on H-MND, compared to 2.7 at% on H-DND, and less than 1% of sp^2 carbon for both types of NDs. Therefore, oxidized and hydrogenated DND and MND behave very similar surface chemistries and mainly differ by their core quality. To be noticed, Miliaieva et al.[28] also reconstructed the energy diagram of Ox-MND and H-MND and evidenced very similar band positioning between Ox-DND and Ox-MND, with a weak shift of 0.1 eV. Though, we performed photocatalysis experiments with both MND surface chemistries, in the same experimental conditions than with DND. When TEOA is used as sacrificial reagent (1 vol%), the hydrogen production rate remains below the TEOA reference whatever the surface chemistry of MND (**Figure 7**). No hydrogen overproduction is measured in presence of Ox-MND while it was the case in strictly similar conditions with Ox-DND. This experiment emphasizes that defects and impurities present in the DND core may play a role in the absorption of visible light and the mechanisms leading to H_2 production.

DND usually contain various chemical impurities (mainly metallic oxides) at the ppm or even at the ppb level,[32] surrounding the particles or embedded in their core. A possible role of these chemical impurities during the photocatalytic experiments needs to be considered. Obviously, impurities embedded in the DND core are unlikely to be significantly involved as the DND of the same source did not exhibit H_2 production after surface hydrogenation. For the impurities surrounding the particles, as the quantification studies revealed that their concentrations in DND are strongly source-dependent,[32] we thus performed a control test, using a second source of detonation nanodiamonds (ADAMAS). Here as well, hydrogen overproduction was only observed with oxidized DND and not with H-DND. This last result allows us to rule out the hypothesis of a phenomenon dependent on the source of DND and reinforces the idea of a specific reactivity of Ox-DND thanks to the conjecture of defects presence in their core, adapted band alignments, and optimized water adsorption at their surface.

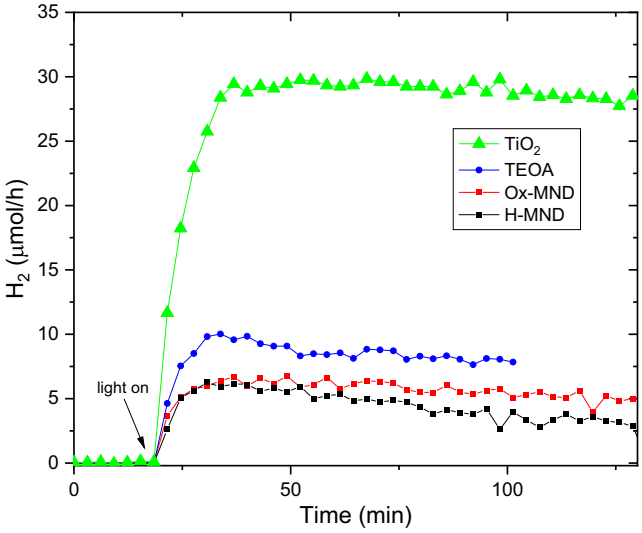

Figure 7. Hydrogen production rate (μmol h^{-1}) for Ox-MND (red squares) and H-MND (black squares) (TEOA: 1 vol%). TiO_2 (green triangles) and TEOA (blue circles) references were added for comparison. 10 mg of Ox-DND and TiO_2 were used.

4. Conclusion

The hydrogen overproduction by oxidized DND suspended in water under solar illumination was highlighted by comparison with the sacrificial reagent alone. This result is obtained without any cocatalyst and/or heterojunction with another semiconductor. Measured performances are at least similar to the TiO_2 P25 reference for the two used sacrificial reagents (TEOA and MeOH). The maximum H_2 amount of 5.2 mmol h^{-1} g^{-1}, obtained for 5 mg of oxidized DND, is comparable to the one obtained from other photocatalysts investigated in the same photocatalytic conditions. From the best of our knowledge, this is the first report for DND alone in these illumination conditions. The surface chemistry of DND plays a crucial role as no hydrogen overproduction is measured for hydrogenated DND from the same source in the same experimental conditions. The possible origin of this hydrogen overproduction was discussed in terms of band diagrams, residual sp^2 carbon, core structural defects and chemical impurities present in DND, and hydrophilicity. Obviously, all these assertions will have to be thoroughly

investigated in further experiments to better understand and maximize the behavior of Ox-DND for hydrogen production. Nevertheless, this novel result opens exciting perspectives for NDs and green hydrogen production.

5. Experimental Section

In this study, DND provided by PlasmaChem (GD02, purity >99.9%) were used. Their specific surface area measured by BET was $297 \pm 30\ m^2\ g^{-1}$. Their size distribution (Feret diameter) measured from transmission electron microscopy images with a statistic of 180 nanoparticles was centered around 6.4 ± 1.6 nm (Figure S1, Supporting Information).

Surface Treatments of DND: Raw DND particles may exhibit nondiamond phases at their surface (amorphous or graphitic carbon), which can be efficiently removed by harsh oxidation treatment,[33] such as an annealing under air at the threshold of the diamond etching temperature (see thermogravimetry analysis, TGA in Figure S2, Supporting Information). 200 mg of DND were then treated at 500 °C under air at atmospheric pressure during 90 min in a tubular furnace (Ox-DND). After this oxidation treatment, some DND were annealed under hydrogen flow (50 sccm) at 750 °C and atmospheric pressure during 5 h (H-DND).

Characterization of the DND Surface Chemistry: X-ray Photoemission Spectroscopy (XPS): Both DND were analyzed by XPS to determine atomic concentrations of chemical elements. A droplet of 10 µL of DND in water was deposited on a silicon substrate covered by a gold layer deposited by evaporation to limit the charge phenomenon during XPS analysis. Substrates were dried and then analyzed. XPS measurements were performed on a Kratos Analytical Axis Ultra DLD spectrometer equipped with a monochromated Al Kα (1486.6 eV) X-ray source and a charge compensation system (Manchester, UK). The take-off angle was set at 90° relative to the sample surface. Spectra were acquired at a pass energy of 160 eV for the survey, 40 eV for core levels (O 1s, N 1s, C 1s). C 1s spectra shown in this study were acquired at 20 eV to reach a higher energy resolution. Valence bands spectra were recorded at a pass energy of 20 eV. Binding energies were referenced to the N 1s peak located at 400.2 eV. After the background subtraction by a Shirley correction, a curve fitting procedure was carried out to extract the components of the C 1s core level using Voigt functions with a Lorentzian to Gaussian ratio of 30%.

Characterization of the DND Surface Chemistry: Fourier Transform Infrared Spectroscopy (FTIR): Infrared spectra were recorded with a Bruker Alpha II spectrometer equipped with a Platinum ATR system (diamond crystal). 2 µL of ND in suspension were deposited on the ATR crystal and allowed to dry under a flow of dry nitrogen ($\approx 1\ L\ min^{-1}$) for few minutes. Spectra acquisition was realized while keeping the nitrogen flow, with a resolution of $4\ cm^{-1}$. Spectra given in the present study are the average of 128 scans for the sample.

Characterization of the DND Surface Chemistry: Raman Spectroscopy: Raman spectra were recorded with a Horiba Xplora spectrometer equipped with a 532 nm laser with a 0.79 mW power (Kyoto, Japan). 10 µL of DND in water were deposited on a silicon substrate and dried. Each spectrum is the average of three acquisitions realized at different positions on the substrate. The acquisition time is 1 min, cumulated 10 times.

Characterization of the DND Surface Chemistry: UV–Vis Spectroscopy: Absorbance measurements were performed with a Shimadzu UV-3600 plus series in a quartz cell with an optical pathway of 1 cm, using diluted suspension at $0.05\ mg\ mL^{-1}$.

Colloidal Properties: Ox-DND and H-DND nanoparticles were suspended in ultra-pure water by sonication at 10 °C for 30 min with a 1 s on/off period and an amplitude of 60% (Cup Horn Bioblock Scientific 750 W) followed by a centrifugation step (2400 g, 40 min). A colloidal suspension concentrated at 1 wt% was obtained. Concentration of colloids was measured by weighting the residue of 100 µL of supernatant dried overnight at room temperature. Mean hydrodynamic diameters of 43 ± 4 and 45 ± 3 nm were measured by dynamic light scattering on the Ox-DND and H-DND suspensions, respectively. Zeta potential measurements exhibited a negative value of -57 ± 5 mV in agreement with the carboxylated surface at this pH and a positive one of $+66 \pm 8$ mV for hydrogenated DND, as expected.[12]

Photocatalytic Experiments: Toward photocatalytic H_2 production experiments, 5, 10, or 20 mg of Ox-DND and H-DND in suspension were diluted into 800 mL of ultra-pure water, resulting in 6.25, 12.5, and 25 $\mu g\ mL^{-1}$ concentrated solutions. TEOA or MeOH was used as an antioxidant (sacrificial reagent) and added to the suspensions at low concentration, lower than the ones currently used for photocatalytic water-splitting, i.e., ranging from 0.1 to 1 vol% for TEOA. Two concentrations of 1 and 10 vol% were investigated for MeOH. Suspensions were then illuminated by a Spalite Hit lamp (G12 8800 K (Art-nr 226 224) of 150 W (irradiance $23.6\ mW\ cm^{-2}$) simulating the solar spectrum (in Figure S3, Supporting Information). Experiments were conducted at ambient temperature under magnetic agitation at 700 rpm and a continuous N_2 flow ($100\ cm^3\ min^{-1}$). On-line hydrogen production yield was monitored by gas chromatography (µGC R-3000 SRA Instrument), with acquisitions repeated every 250 s. To benchmark Ox-DND and H-DND performances, commercial TiO_2 particles (P25, Evonik) suspended in ultra-pure water were illuminated in similar conditions.

Supporting Information

Supporting Information is available from the Wiley Online Library or from the author.

Acknowledgements

Authors would like to acknowledge the French Alternative Energies and Atomic Energy Commission (CEA) for the funding of L.S., Ph.D. Authors would like also to thank Jocelyne Leroy for XPS measurements.

Conflict of Interest

The authors declare no conflict of interest.

Data Availability Statement

The data that support the findings of this study are available from the corresponding author upon reasonable request.

Keywords

hydrogen production, metal-free photocatalysts, nanodiamonds, solar irradiation, surface chemistry

Received: November 30, 2023
Revised: December 11, 2023
Published online:

[1] N. Nunn, M. Torelli, G. McGuire, O. Shenderova, *Curr. Opin. Solid State Mater. Sci.* **2017**, *21*, 1.
[2] S. Navalón, A. Dhakshinamoorthy, M. Álvaro, H. García, *Chem. Mater.* **2020**, *32*, 4116.
[3] P. Shao, J. Tian, F. Yang, X. Duan, S. Gao, W. Shi, X. Luo, F. Cui, S. Luo, S. Wang, *Adv. Funct. Mater.* **2018**, *28*, 1705295.
[4] L. Zhang, R. J. Hamers, *Diamond Relat. Mater.* **2017**, *78*, 24.
[5] W. A. Maza, V. M. Breslin, T. I. Feygelson, P. A. DeSario, B. B. Pate, J. C. Owrutsky, A. Epshteyn, *Appl. Catal., B* **2023**, *325*, 122306.

[6] L. X. Su, Z. Y. Liu, Y. L. Ye, C. L. Shen, Q. Lou, C. X. Shan, *Int. J. Hydrogen Energy* **2019**, *44*, 19805.
[7] Z. Lin, J. Xiao, L. Li, P. Liu, C. Wang, G. Yang, *Adv. Energy Mater.* **2016**, *6*, 1501865.
[8] D. M. Jang, Y. Myung, H. S. Im, Y. S. Seo, Y. J. Cho, C. W. Lee, J. Park, A. Y. Jee, M. Lee, *Chem. Commun.* **2012**, *48*, 696.
[9] O. A. Shenderova, G. E. McGuire, *Biointerphases* **2015**, *10*, 030802.
[10] S. Turner, O. Shenderova, F. Da Pieve, Y. G. Lu, E. Yücelen, J. Verbeeck, D. Lamoen, G. Van Tendeloo, *Phys. Status Solidi A* **2013**, *210*, 1976.
[11] C. Bradac, S. Osswald, *Carbon* **2018**, *132*, 616.
[12] J. C. Arnault, H. A. Girard, *Curr. Opin. Solid State Mater. Sci.* **2017**, *21*, 10.
[13] F. Ducrozet, H. A. Girard, J. Leroy, E. Larquet, I. Florea, E. Brun, C. Sicard-Roselli, J. C. Arnault, *Nanomaterials* **2021**, *11*, 2671.
[14] E. Mayerhoefer, A. Krueger, *Acc. Chem. Res.* **2022**, *55*, 3594.
[15] T. Petit, M. Pfluger, D. Tolksdorf, J. Xiao, E. F. Aziz, *Nanoscale* **2015**, *7*, 2987.
[16] T. Petit, L. Puskar, T. Dolenko, S. Choudhury, E. Ritter, S. Burikov, K. Laptinskiy, Q. Brzustowski, U. Schade, H. Yuzawa, M. Nagasaka, N. Kosugi, M. Kurzyp, A. Venerosy, H. Girard, J. C. Arnault, E. Osawa, N. Nunn, O. Shenderova, E. F. Aziz, *J. Phys. Chem. C* **2017**, *121*, 5185.
[17] S. L. Y. Chang, P. Reineck, D. Williams, G. Bryant, G. Opletal, S. A. El-Demrdash, P. L. Chiu, E. Osawa, A. S. Barnard, C. Dwyer, *Nanoscale* **2020**, *12*, 5363.
[18] E. Brun, H. A. Girard, J. C. Arnault, M. Mermoux, C. Sicard-Roselli, *Carbon* **2020**, *162*, 510.
[19] J. C. Arnault, *Diamond Relat. Mater.* **2018**, *84*, 157.
[20] S. Turner, O. I. Lebedev, O. Shenderova, I. I. Vlasov, J. Verbeeck, G. Van Tendeloo, *Adv. Funct. Mater.* **2009**, *19*, 2116.
[21] J. I. B. Wilson, J. S. Walton, G. Beamson, *J. Electron Spectrosc. Relat. Phenom.* **2001**, *121*, 183.
[22] L. Saoudi, H. A. Girard, E. Larquet, M. Mermoux, J. Leroy, J. C. Arnault, *Carbon* **2023**, *202*, 438.
[23] T. Petit, L. Puskar, *Diamond Relat. Mater.* **2018**, *89*, 52.
[24] I. Bydzovska, E. Shagieva, I. Gordeev, O. Romanyuk, Z. Nemeckova, J. Henych, L. Ondic, A. Kromka, S. Stehlik, *Nanomaterials* **2021**, *11*, 2251.
[25] S. Stehlik, J. Henych, P. Stenclova, R. Kral, P. Zemenova, J. Pangrac, O. Vanek, A. Kromka, B. Rezek, *Carbon* **2021**, *171*, 230.
[26] M. Mermoux, A. Crisci, T. Petit, H. A. Girard, J. C. Arnault, *J. Phys. Chem. C* **2014**, *118*, 23415.
[27] C. Marchal, T. Cottineau, M. G. Méndez-Medrano, C. Colbeau-Justin, V. Caps, V. Keller, *Adv. Energy Mater.* **2018**, *8*, 1702142.
[28] D. Miliaieva, A. Sokeng Djoumessi, J. Čermák, K. Kolarova, M. Schaal, F. Otto, E. Shagieva, O. Romanyuk, J. Pangrác, J. Kulicek, V. Nádaždy, S. Stehlik, A. Kromka, H. Hoppe, B. Rezek, *Nanoscale Adv.* **2023**, *5*, 4402.
[29] P. Jiménez-Calvo, V. Caps, M. N. Ghazzal, C. Colbeau-Justin, V. Keller, *Nano Energy* **2020**, *75*, 104888.
[30] F. Buchner, T. Kirschbaum, A. Venerosy, H. Girard, J. C. Arnault, B. Kiendl, A. Krueger, K. Larsson, A. Bande, T. Petit, C. Merschjann, *Nanoscale* **2022**, *14*, 17188.
[31] S. Stehlik, T. Glatzel, V. Pichot, R. Pawlak, E. Meyer, D. Spitzer, B. Rezek, *Diamond Relat. Mater.* **2016**, *63*, 97.
[32] D. P. Mitev, A. T. Townsend, B. Paull, P. N. Nesterenko, *Carbon* **2013**, *60*, 326.
[33] E. Nehlig, S. Garcia-Argote, S. Feuillastre, M. Moskura, T. Charpentier, M. Schleguel, H. A. Girard, J. C. Arnault, G. Pieters, *Nanoscale* **2019**, *11*, 8027.